Unconventional Superfluid Order in the F Band of a Bipartite Optical Square Lattice

Matthias Ölschläger, Georg Wirth, and Andreas Hemmerich

Institut für Laser-Physik, Universität Hamburg, Luruper Chaussee 149, 22761 Hamburg, Germany

(Received 27 August 2010; revised manuscript received 3 December 2010; published 6 January 2011)

We report on the first observation of bosons condensed into the energy minima of an F band of a bipartite square optical lattice. Momentum spectra indicate that a truly complex-valued staggered angular momentum superfluid order is established. The corresponding wave function is composed of alternating local $F_{2x^3-3x} \pm iF_{2y^3-3y}$ orbits and local S orbits residing in the deep and shallow wells of the lattice, which are arranged as the black and white areas of a checkerboard. A pattern of staggered vortical currents arises, which breaks time-reversal symmetry and the translational symmetry of the lattice potential. We have measured the populations of higher order Bragg peaks in the momentum spectra for varying relative depths of the shallow and deep lattice wells and find remarkable agreement with band calculations.

DOI: 10.1103/PhysRevLett.106.015302 PACS numbers: 67.85.−d, 03.75.Hh, 03.75.Lm, 37.10.Jk

Orbital physics plays a central role for magnetism, superconductivity, and transport properties of rare earth and transition metal compounds including high T_c cuprate systems or heavy fermion systems, which have been a subject of intense research for more than two decades [1,2]. The advent of optical lattices (i.e., quantum gases arranged in synthetic lattices formed by light) has raised hopes that certain aspects of such systems could be studied in a precisely controlled environment without many of the complexities usually associated with material systems [3,4]. Unfortunately, the wave function of bosons in their ground state is positive definite under very general circumstances [5,6], which significantly limits their usefulness for simulating many-body systems of interest. Fermions, on the other hand, are significantly harder to prepare in optical lattices [7,8] and the realization of large filling factors required to access orbital physics at large angular momenta appears difficult, if not impossible. This has recently triggered extensive theoretical research driven by the vision to explore orbital physics with bosons via targeted population of higher bands [9–13]. Interesting many-body phenomena were predicted including supersolid quantum phases in cubic lattices [14,15], quantum stripe ordering in triangular lattices [16], flat bands and Wigner crystallization in honeycomb lattices [17], or incommensurate superfluidity, which spontaneously breaks time-reversal, rotational, and translational symmetries [18]. These and many other exciting proposals all rely upon the requirement that higher bands could be selectively populated and cross-dimensional coherence could be established. Clever new techniques have recently made it possible to populate the P band [19–22]. However, the D and F bands in optical lattices with their particular relevance in condensed matter systems have remained practically unexplored by experiments.

In this Letter we report the first observation of bosons condensed in the F band of a two-dimensional (2D) bipartite optical lattice. Full cross-dimensional coherence with a lifetime on the order of 10 ms is established. The observed momentum spectra exhibit a characteristic pattern of sharp maxima, which are well explained by a complex-valued superfluid order parameter composed of alternating local $F_{2x^3-3x} \pm iF_{2y^3-3y}$ orbits and local S orbits. A pattern of staggered local angular momenta and staggered vortical currents arises commensurable with the plaquettes of the lattice with the consequence of broken time-reversal symmetry. The proposed nature of the superfluid order (representing a remarkable example beyond Feynmans no-node theorem [5,6]) is confirmed by evaluating the Bloch functions corresponding to the observed condensation quasimomenta. We find remarkable agreement of the observed momentum spectra with calculations based upon these Bloch functions.

By crossing two optical standing waves derived from laser beams with 100 μm $1/e^2$ radius and a wavelength $\lambda = 1064$ nm, we produce a (quasi-2D) light shift potential

$$V(x,y) \equiv -\frac{V_0}{4} e^{-(2z^2/w_0^2)} |\eta(e^{ikx} + \epsilon e^{-ikx}) + e^{i\theta}(e^{iky} + \epsilon e^{-iky})|^2, \quad (1)$$

providing two classes of (tube-shaped) lattice sites (denoted as $\mathcal{A}$ and $\mathcal{B}$) arranged as shown in Fig. 1(a). Here, $k \equiv 2\pi/\lambda$, η is experimentally adjustable (around unity) and ϵ is fixed to ≈ 0.9 due to imperfect reflection optics used in the experiment. For details we refer to Ref. [22]. Adjustment of the parameter θ lets us tune the difference of the well depths of $\mathcal{A}$ and $\mathcal{B}$ sites. For $\theta < \pi/2$ the $\mathcal{A}$ sites are more shallow than the $\mathcal{B}$ sites and vice versa.

An efficient population of excited bands is obtained by optimizing a population swapping procedure described in more detail in Ref. [22]. Initially a Bose-Einstein condensate of Rubidium (^{87}Rb) atoms is prepared at a temperature of about 70 nK ($\approx 0.7T_c$) and the lattice potential is ramped up within 80 ms to $V_0/E_{\mathrm{rec}} = 16.6$ for a value

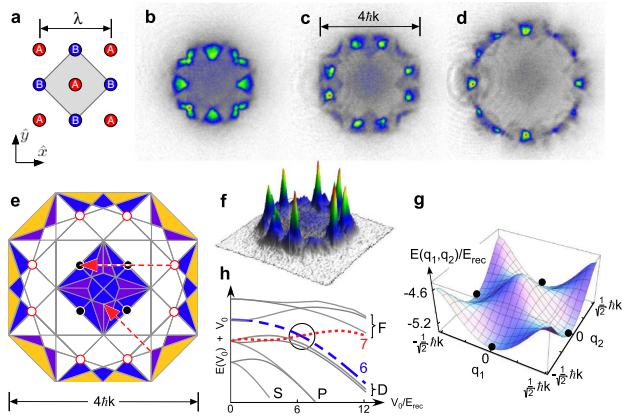

FIG. 1 (color online). (a) The bipartite lattice comprises two classes of lattice sites denoted by $\mathcal{A}$ and $\mathcal{B}$. The grey area shows the Wigner-Seitz unit cell of the $\mathcal{A}$ sublattice. (b), (c), and (d) Observed populations of Brillouin zones (BZs) after applying the population swapping procedure with final values of $(\theta/\pi, V_0/E_{\mathrm{rec}}) = (0.61, 5.8)$, $(0.66, 8.3)$, $(0.69, 13.3)$, respectively. (e) Schematic of the 6th [dark (blue and purple) areas] and 7th [light (orange) areas] BZs. The eight open (red) circles mark the points, where the atoms are observed to gather in (c). In the center, the first BZ is reconstructed by translations of subsets of the 6th BZ via reciprocal lattice vectors indicated by the (red) dashed arrows. (f) 3D representation of the image in (c). (g) energy surface of the 7th band with degenerate minima indicated by filled black circles corresponding to those in (e). (h) Band energies E at $\mathbf{K}_{(1,1)}$ versus the well depth V_0. The black circle indicates a crossing of the 7th [dotted (red) line] and the 6th [dashed (blue) line] bands.

$\theta < \pi/2$ such that the well depth of the $\mathcal{B}$ sites significantly exceeds that of the $\mathcal{A}$ sites ($E_{\mathrm{rec}} \equiv \hbar^2 k^2/2m$ denotes the recoil energy with the atomic mass m). A ground state lattice is thus formed with most atoms residing in the deeper $\mathcal{B}$ wells. The large well depth yields nearly complete suppression of tunneling. Subsequently θ is rapidly changed (within 0.2 ms, which is shorter than the nearest neighbor tunneling time) to a final value θ_f above $\pi/2$ such that now the $\mathcal{A}$ wells are significantly deeper than the $\mathcal{B}$ wells. Finally, V_0 is adiabatically decreased during 0.6 ms to admit tunneling again. Optionally a 2 ms long phase is appended, where θ is adiabatically tuned to some desired value followed by a variable hold time.

In Figs. 1(b)–1(d) the population of different bands is illustrated. To obtain these pictures, population swapping is carried out with θ_f and V_0 optimized for maximal population of the desired band. The lattice beam intensity is then exponentially decreased with a time constant of 430 μs and after 30 ms absorption imaging is applied. This yields images of momentum space, where the population $P[n, q]$ in the nth band for some quasimomentum q and energy $E[n, q]$ is mapped to some point within the nth Brillouin zone (BZ) related to q by a reciprocal lattice vector. This mapping requires that $E[n, q]$ does not cross some other $E[n', q]$ during the adiabatic switch off process. As a consequence of such band crossings a part of the band population may be mapped to an adjacent BZ. The image in Fig. 1(b) (with $\theta/\pi = 0.61$ and $V_0/E_{\mathrm{rec}} = 5.8$) matches well with the 4th BZ, while in Fig. 1(d) (with $\theta/\pi = 0.69$ and $V_0/E_{\mathrm{rec}} = 13.3$) the 9th BZ is found to be the most populated. This directly indicates the numbers of the bands that have been populated to be $n = 4$ and $n = 9$, respectively.

For the case of interest in this Letter in Fig. 1(c), where $\theta/\pi = 0.66$ and $V_0/E_{\mathrm{rec}} = 8.3$, the assignment of a single BZ is not possible. Instead the atoms share the 6th and 7th BZ with emphasis on the 6th BZ. This is illustrated by Fig. 1(e), where the shapes of the 6th [dark (blue and purple)] and 7th [light (orange)] BZs are sketched. One recognizes in Fig. 1(c) and 1(f) that the BZs are not evenly populated but rather a large fraction of the atoms accumulate at eight quasimomenta at the inner boundary of the 6th BZ highlighted by the open (red) circles in Fig. 1(e). These atoms can be identified to reside at the minima of the energy surface of the 7th band (i.e., the lowest of the four possible F bands). In Fig. 1(g) we show a plot of this band derived from a band calculation involving a Fourier expansion of the Bloch functions with 11 harmonics in each dimension and the potential of Eq. (1). Indicated in Fig. 1(g) by filled black circles, four local minima of the energy surface arise at the quasimomenta $\mathbf{K}_{(1,1)}$, $\mathbf{K}_{(-1,-1)}$, $\mathbf{K}_{(1,-1)}$, $\mathbf{K}_{(-1,1)}$, where $\mathbf{K}_{(\nu,\mu)} \equiv \frac{1}{2}\hbar k(\nu\hat{x} + \mu\hat{y})$ with integers ν, μ and $\hat{x}$, $\hat{y}$ denoting the unit vectors in x and y directions. We interpret the accumulation of atoms in the band minima as a result of a condensation process induced by tunneling and collisions, which transfer energy into the third dimension perpendicular to the lattice, which is only weakly confined by the external trap potential (40 Hz trap frequency). Our band calculation also shows that, when V_0 is ramped to zero, a crossing between the 7th and the 6th band occurs for quasimomenta in the vicinity of these energy minima [cf. Fig. 1(h)]. Thus, the energy minima of the 7th band are mapped into the 6th rather than the 7th BZ. The equivalence of the open (red) circles in Fig. 1(e) and the filled black circles in Fig. 1(g) is shown in the BZ illustration in Fig. 1(e), where the 6th BZ is mapped onto the first BZ via translations with reciprocal lattice vectors [indicated by the (red) dashed arrows].

In Figs. 2(a)–2(c) momentum spectra are shown for a hold time in the lattice of 1 ms, a well depth parameter $V_0/E_{\mathrm{rec}} = 8.3$ and $\theta/\pi = 0.66$, 0.70, 0.75, respectively. The upper row shows the experimental observations obtained by rapidly (< 1 μs) switching off the lattice potential and absorption imaging after 30 ms of ballistic expansion. The presence of sharp Bragg peaks at quasimomenta $\mathbf{K}_{(\nu,\mu)}$ for odd integers ν, μ clearly demonstrates cross-dimensional coherence. One recognizes the absence of a zero momentum component ($\nu = \mu = 0$). In fact, the lowest order components arise at the condensation points in Fig. 1(g). Limited by the finite expansion time, the

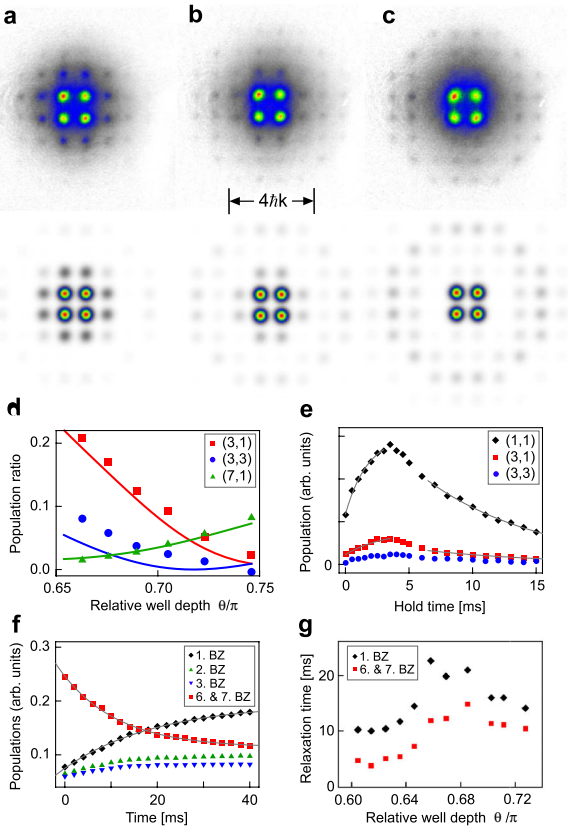

FIG. 2 (color online). In (a), (b), and (c) momentum spectra are shown for a hold time of 1 ms, $V_0/E_{\mathrm{rec}} = 8.3$ and $\theta/\pi = 0.66$, 0.70, 0.75, respectively. Observations (calculations) are shown in the upper (lower) row. (d) Population ratio for higher order and zero order Bragg peaks plotted versus θ. Observations (calculations) are shown by the symbols (solid lines). (e) Temporal evolution of the populations of Bragg peaks. The solid lines are exponential fits applied in the wings of the graphs to determine relaxations times. (f) Temporal evolution of band populations for $V_0/E_{\mathrm{rec}} = 8.3$ and $\theta/\pi = 0.67$. The solid lines are exponential fits. (g) $1/e$ times for depopulation of the 6th and 7th BZ and repopulation of the 1st BZ plotted versus θ.

interaction energy and finite imaging resolution, the widths of the observed Bragg peaks set a lower bound of the coherence area of 3 μm $\times$ 3 μm, which is to be compared to the sample size of about 20 μm $\times$ 20 μm. The kinetic energy within the lattice plane exceeds the collision energy per particle ($\approx E_{\mathrm{rec}}$) such that a description of the band structure in terms of single particle Bloch functions appears justified. The lower rows in Figs. 2(a)–2(c) show calculations of momentum spectra of the coherent superposition $\Psi_F \equiv \phi_{\mathbf{K}_{(1,1)}} + c\phi_{\mathbf{K}_{(1,-1)}}$ of the real-valued Bloch functions corresponding to the two inequivalent condensation points. Only for choices of "c" close to the values "$\pm i$" good agreement with the observations is found. In Fig. 2(d) the θ dependence is studied more quantitatively. In this graph the symbols show the population ratios between higher order $[(\nu, \mu) = (3, 1), (3, 3), (7, 1)]$ Bragg peaks and the zero order Bragg peak $((\nu, \mu) = (1, 1))$ observed for varying values of θ. The peak populations are obtained by counting the number of atoms in a small circular region covering an individual Bragg peak and subtracting the number of atoms found in a surrounding ring-shaped area of the same size. The theoretical curves (solid lines) do not involve any free parameters.

In Fig. 2(e) we study the time scales for the formation and the decay of coherence by evaluating momentum spectra at fixed values $V_0/E_{\mathrm{rec}} = 8.3$ and $\theta/\pi = 0.66$ for different holding times. The graph shows the Bragg peak populations [obtained as in (d)] for the peaks identified in the inset. During the first few milliseconds, which amounts to a few tunneling times (≈ 1 ms), all peak populations increase before decay sets in with a time scale corresponding to the collisional relaxation of the band populations, which exceeds the on-site collision time (≈ 0.1 ms) by nearly 2 orders of magnitude. Both time scales are determined by exponential fits as 1.8 ms and 9.1 ms for the zero order peak (black diamonds) and 2.9 ms and 10.1 ms for the first order peak identified by red rectangles.

To investigate collision-induced band relaxation, in Fig. 2(f) the fraction of atoms found in the different BZs after population of the 7th band are plotted versus the hold time for $V_0/E_{\mathrm{rec}} = 8.3$ and $\theta/\pi = 0.67$. The 4th and the 5th BZ, which maintain nearly constant population during the observation time, have been omitted for better legibility. The initially prepared population in the 6th and 7th BZ decays and the 1st BZ is repopulated. The corresponding relaxation times are determined by means of exponential fits (solid lines) to be 12.3 ms and 19.9 ms, respectively, which are 2 orders of magnitude larger than the estimated collision time. Similarly, the relaxation times for other values of θ are determined and plotted in Fig. 2(g). One recognizes that around $\theta/\pi \approx 0.68$ the relaxation times attain maximal values. The local S orbits of the wave function Ψ_F (a detailed discussion of its geometry follows below) become maximally developed for this setting of θ. Because the ground state wave function has vanishing amplitude in the shallow wells, its overlap with Ψ_F is reduced for this case, and thus collisional decay into the ground state is inhibited.

The wave function Ψ_F has remarkable properties illustrated in Fig. 3, where its local amplitude (grey areas indicate large amplitude) and phase [(colored) numbers] is sketched. In the deep wells Ψ_F resembles the superposition $\psi_{[3,0]} \pm i\psi_{[0,3]}$ of eigenfunctions $\psi_{[n,m]}$ of a 2D harmonic oscillator with n, m oscillator quanta in x and y directions, which display a spatial $(2x^3 - 3x) \pm i(2y^3 - 3y)$ dependence at the well center. The relative phases "$\pm i$" maximize the local angular momentum yielding a maximally isotropic shape of the local F orbits, such that the atoms (which interact repulsively) can best avoid each other. This minimizes the mean field energy and hence Ψ_F represents the true ground state of the F band. For P orbits a similar prediction is discussed in Refs. [9,10].

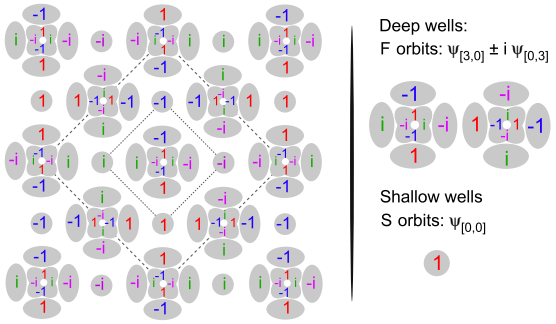

FIG. 3 (color online). Orbit configuration of order parameter Ψ_F. The grey areas characterize the antinodal structure of the orbits, the (colored) numbers indicate the local phases.

In contrast, in the shallow wells, Ψ_F mimics the harmonic oscillator S orbit $\psi_{[0,0]}$. The checkerboardlike arrangement of S orbits and F orbits with alternating angular momentum provides equal local phases on both sides of the tunneling junctions and thus maximizes the tunneling efficiency. The inner and outer dashed rectangles denote the unit cells of the lattice and of Ψ_F, respectively. The sublattice of shallow wells possesses a pattern of staggered vortical currents commensurate with its plaquette structure, which match with the alternating orbital currents in the deep wells. As a consequence Ψ_F breaks the translation symmetry of the lattice and time-reversal symmetry. Order parameters with similar properties have been recently predicted in the ground states of driven optical lattices [23,24].

Finally, the assumption of an incoherent mixture of phases $\phi_{\mathbf{K}_{(1,1)}}$ and $\phi_{\mathbf{K}_{(1,-1)}}$ would necessarily imply their spatial separation, since at the shallow wells both Bloch functions share common local S orbits. A phase separation scenario, however, requires excess kinetic energy at the phase boundaries due to inhibited tunneling and excess mean field energy. A compensating local anisotropy, sufficient to enforce local condensation in a single condensation point, is not available in our experiment. The band minima are found to coincide in their energies to better than $10^{-3}E_{\mathrm{rec}}$ for a wide range of settings of ϵ and η in Eq. (1). This should be compared to the collision energy per particle in the F band estimated to be on the order of E_{rec}. We thus may conclude that the small local imbalance of the standing wave intensities ($< 10\%$), which is unavoidable due to the use of finite-sized Gaussian beams and a finite-sized atomic sample, does not notably lift the degeneracy. Also the underlying harmonic trap should not favor phase separation since $\phi_{\mathbf{K}_{(1,1)}}$ and $\phi_{\mathbf{K}_{(1,-1)}}$ experience the same trapping potential. A quantitative discussion of phase separation for our system requires theoretical efforts beyond the scope of the present work. Our theoretical considerations are for zero effective temperature of the atoms within the F band. Accounting for finite-temperature effects is conceptually difficult since the system resides in a metastable state. Stringent measurement schemes for the temperature in optical lattices are a subject of an ongoing debate even in the ground state [25]. A direct observation of the staggered orbital order could be possibly achieved with detection schemes operating in configuration space with single site resolution as recently developed by several groups [26].

We are grateful to C. Morais Smith and L.-K. Lim for fruitful discussions. This work was partially supported by DFG (He2334/10-1, GrK 1355) and the Excellence cluster ''Frontiers in Quantum Photon Science''.

[1] Y. Tokura and N. Nagaosa, Science **288**, 462 (2000).
[2] S. Maekawa *et al.*, *Physics of Transition Metal Oxides*, Springer Series in Solid-State Sciences Vol. 144 (Springer, New York, 2004).
[3] M. Lewenstein *et al.*, Adv. Phys. **56**, 243 (2007).
[4] I. Bloch, J. Dalibard, and W. Zwerger, Rev. Mod. Phys. **80**, 885 (2008).
[5] R. P. Feynman, *Statistical Mechanics: A Set of Lectures* (Addison-Wesley, Reading, MA, 1972).
[6] C. Wu, Mod. Phys. Lett. B **23**, 1 (2009).
[7] M. Köhl *et al.*, Phys. Rev. Lett. **94**, 080403 (2005).
[8] J. K. Chin *et al.*, Nature (London) **443**, 961 (2006).
[9] A. Isacsson and S. M. Girvin, Phys. Rev. A **72**, 053604 (2005).
[10] W. V. Liu and C. Wu, Phys. Rev. A **74**, 013607 (2006).
[11] A. B. Kuklov, Phys. Rev. Lett. **97**, 110405 (2006).
[12] C. Xu and M. P. A. Fisher, Phys. Rev. B **75**, 104428 (2007).
[13] J. Larson, A. Collin, and J.-P. Martikainen, Phys. Rev. A **79**, 033603 (2009).
[14] V. W. Scarola and S. Das Sarma, Phys. Rev. Lett. **95**, 033003 (2005).
[15] V. W. Scarola, E. Demler, and S. Das Sarma, Phys. Rev. A **73**, 051601(R) (2006).
[16] C. Wu *et al.*, Phys. Rev. Lett. **97**, 190406 (2006).
[17] C. Wu *et al.*, Phys. Rev. Lett. **99**, 070401 (2007).
[18] V. M. Stojanović *et al.*, Phys. Rev. Lett. **101**, 125301 (2008).
[19] A. Browaeys *et al.*, Phys. Rev. A **72**, 053605 (2005).
[20] T. Müller *et al.*, Phys. Rev. Lett. **99**, 200405 (2007).
[21] M. Anderlini *et al.*, Nature (London) **448**, 452 (2007).
[22] G. Wirth, M. Ölschläger, and A. Hemmerich, arXiv:1006.0509v3 [Nature Phys. (to be published)].
[23] A. Hemmerich and C. M. Smith, Phys. Rev. Lett. **99**, 113002 (2007).
[24] L.-K. Lim, C. M. Smith, and A. Hemmerich, Phys. Rev. Lett. **100**, 130402 (2008).
[25] Q. Zhou and T.-L. Ho, arXiv:0908.3015v2.
[26] W. S. Bakr *et al.*, Nature (London) **462**, 74 (2009).